Prince JA, Bhuvana S, Anbharasi V, Ayyanar N, Boodhoo KVK, Singh G.

Ultra-wetting graphene-based membrane.

***Journal of Membrane Science* 2016, 500, 76-85.**

Ultra-wetting graphene-based membrane

J.A. Prince, S. Bhuvana, V. Anbharasi, N. Ayyanar, K.V.K. Boodhoo, G. Singh

www.elsevier.com/locate/memsci

PII: S0376-7388(15)30324-0
DOI: http://dx.doi.org/10.1016/j.memsci.2015.11.024
Reference: MEMSCI14117

To appear in: *Journal of Membrane Science*

Received date: 3 August 2015
Revised date: 17 November 2015
Accepted date: 19 November 2015

Cite this article as: J.A. Prince, S. Bhuvana, V. Anbharasi, N. Ayyanar, K.V.K. Boodhoo and G. Singh, Ultra-wetting graphene-based membrane, *Journal o Membrane Science,* http://dx.doi.org/10.1016/j.memsci.2015.11.024

Ultra-wetting graphene-based membrane

J. A. Prince [a, b,] *, S. Bhuvana[a], V. Anbharasi[a], N. Ayyanar[a],K.V.K. Boodhoo[b]and G. Singh[a,]*

[a]Environmental and Water Technology Centre Of Innovation (EWTCOI), Ngee Ann Polytechnic, Singapore 599489

[b] School of Chemical Engineering and Advanced Materials, Faculty of Science, Agriculture and Engineering, Newcastle University, Newcastle upon Tyne, NE1 7RU, United Kingdom

*Corresponding author: J. A. Prince: jap2@np.edu.sg / G. Singh: sgu3@np.edu.sg

Keywords: (Ultra-wetting graphene, graphene membrane, graphene nanocomposite, ultrafiltration, zero contact angle, functionalized graphene)

ABSTRACT:

Carbon nanomaterials such as graphene and its derivatives based membranes in real applications are still far from reality due to their hydrophobic nature and limitations in their fabrication process. Here, we have devised a simple and feasible fabrication method to bring the high end nanocarbon based material to real downstream applications. In order to achieve this objective, the wettability of graphene was initially increased to an ultra-wetting level by incorporating amine and carboxyl functionality onto the graphene. The amine and carboxylated graphene is then covalently attached to a polymer matrix to fabricate a water filtration membrane. The characterization of the modified supported graphene-based membrane indicates that significantly higher hydrophilicity than previously expected is achieved, with the water contact angle reduced to zero. The ultra-wetting graphene increases the water permeability of the membrane by 126% without any changes in the selectivity. Based on our findings, we conclude that the ultra-wetting graphene will be an ideal material for new generation water filtration membranes.

INTRODUCTION:

Graphene is a sp2-hybridized two-dimensional carbon sheet [1] which has been used for several promising applications such as energy storage [2], surface coating [3-6], nanopore sequencing [7] and filtration [8]. The wetting behaviour of graphene plays an important role in these applications in addition to its energy storage efficiency and heat transfer capacity [9, 10]. Recently, graphene gained much attention in the field of membrane science and engineering due to its high surface area [11], high mechanical strength [12] and chemical stability [13]. Theoretical analysis have also predicted that graphene based membranes may exhibit orders of

magnitude greater permeability than the current state of the art membranes [14, 15]. However, most of these studies are based on a single layer of graphene sheet [16]. Experimental studies also show that it is difficult to fabricate leak-free porous graphene membranes with large surface area [7, 17]. Moreover, it is commonly accepted that supported graphene is hydrophobic in nature and its water contact angle is, to some extent, higher than that of graphite [10, 18, 19].These limitations of graphene have led to the development of graphene oxide (GO) which is an amphiphilic graphene derivative (a single-atom layer of graphene) with oxygen containing functional groups (-OH, -COOH) attached to both sides of the graphene flake [20-23]. There are important beneficial aspects to having these oxygen containing functional groups attached to the graphene structure. Firstly, they impart polarity to the flake so that the graphene oxide is able to be more uniformly dispersed in solvents and eventually in the polymer matrix it is blended into [20, 24]. Further, these oxygen containing hydrophilic functional groups improve the wetting properties (hydrophilic properties) of the normally hydrophobic polymeric membranes through hydrogen bonding [25]. Indeed, literature reports that the contact angle of water on pristine graphene oxide films can vary from 0 to 60 degrees [26-28].

Graphene oxide-based membranes exhibit promising qualities in the field of desalination [29] and selective ion penetration [30]. Graphene oxide-polymer hybrid material based membranes also exhibit excellent antifouling property [31] due to the interaction of contaminants with the delocalized p-electrons of the nanocarbons [32-34]. In general, highly hydrophilic polymeric materials will have low mechanical and thermal stability and swell during continuous immersion in water [35].Thermal and mechanical properties of the polymeric membranes is increased by the addition of graphene and its derivatives [36] which imparts a strong rigid structure to the membrane material [12]. Recently graphene oxide (GO) are also being cross linked with polymer

matrix to fabricate membranes and these membranes gives higher permeability [37] and selectivity [38]. In addition to high permeability and selectivity, the dispersion [39] and mechanical properties were also improved significantly by grafting GO with polymer matrix [40].

In this work, we report a facile method to fabricate graphene-based composite membrane in real downstream application. In order to achieve this, the wettability of exfoliated graphene nano platelets (xGnP) will be increased by amination ($-NH_2$) and carboxylation (-COOH) to an ultra-wetting level. While graphene oxide attains an increased level of hydrophilicity via –COOH and –OH functional groups, in this work we chose a combination of –COOH and $–NH_2$ functional groups instead to modify the graphene for use in water filtration membrane applications. Amine modified graphene has recently been reported as an alternative to graphene oxide in biomedical [41] and energy [42] (battery) related applications. Carboxylic and amine functional groups have been shown to give significant improvements in the hydrophilicity of the membranes [25, 43-46] by inter molecular hydrogen bonding [25, 43, 47, 48].The novelty in the present work is that, in addition to improved hydrophilicity due to the presence of amine and acid functional groups, the ultra-wetting modified graphene will also be covalently attached to an anhydride containing polymer matrix namely poly acrylonitrile-co-maleic anhydride (PANCMA) via a simple condensation reaction to form poly amicacid. This is made possible by the terminal $–NH_2$ groups of the functionalised graphene which are known to react readily with anhydrides to form strong, stable covalent bonds. The ultra-wetting graphene attached PANCMA will be thermally imidized to produce the final graphene-poly(acrylonitrile-co-maleimide) (G-PANCMI) polymer composite, which by virtue of the imide functionality, will have improved thermal and chemical

stability. The ultra-wetting graphene modified G-PANCMI so formed will be used to fabricate water filtration membrane by the simple phase inversion method [49, 50].

EXPERIMENTAL:

Materials: Acrylonitrile, maleic anhydride, ethylene diamine and azobisisobutyronitrile (AIBN) were purchased from Sigma Aldrich with 99% purity. High purity ethanol, nitric acid (HNO_3), sulphuric acid (H_2SO_4), thionyl chloride ($SOCl_2$), N-N-Dimethyl acetamide (DMAc) and Fluorescein isothiocyanate (FITC) attached bovine serum albumin (BSA) were also purchased from Sigma Aldrich and used as received. The exfoliated graphene nanoplatelets (xGnP) were purchased from XG Sciences. The water used for the reaction was distilled and de-ionized (DI) with a Milli-Q plus system from Millipore, Bedford, MA, USA.

Methodology:

The membranes were characterized using Fourier Emission Scanning Electron Microscopy (FESEM) to observe the morphology of the samples. The samples were sputter coated with platinum, using a JFC-1600 auto fine coater (JOEL, Tokyo Japan) and the morphology was observed by using FESEM (JOEL JMS-6400, Japan) at different magnifications to calculate the diameter of the fibers. The elemental composition of the xGnP and G-PANCMI was studied using the energy dispersive X-ray (EDX) analysis.

The structure of the xGnP, modified xGnP, PANCMA AND G-PANCMI were investigated by using Fourier transform infrared (FTIR) spectroscopy (FTIR8400, Shimadzu, Japan). The spectra were measured in the transmittance mode from the wave number range 4000 – 450 cm^{-1} with 45 scans.

The surface zeta potential of membranes was measured by the Surpass electro kinetic analyzer (Anton Paar Corporation). The measurements were based on the streaming potential and streaming current and are related to the surface charge at a solid/liquid interface. The zeta potential measurements also indicate the surface chemistry (pH titration) and liquid phase adsorption processes. The membrane was cut to 2cm by 5cm dimension and placed in the clamping cell with two spacers. Here, 500mL of 1mM aqueous potassium chloride solution was supplied to cell as the background electrolyte and 0.25M HCl (acid) and 0.1M KOH were chosen for titration. The acid and the base volume increments were set to 0.1ml. The zeta potential was measured each time starting from pH of around 5 up to 9.5 (for basic range) and then after two times rinsing with MQ water from pH down to 2 (for acidic range). For each pH, the zeta potential measurement was repeated 4 times (2 measurements from left to right and another 2 from right to left) and average was taken.

The water contact angles (CA) of the membranes were determined using the VCA Optima Surface Analysis System (AST Products, Inc., Billerica, MA, USA) to study their hydrophobicity/hydrophilicity. Samples of 4 cm^2 area (2 × 2 cm) at random positions were prepared from each membrane. The samples were then placed on the glass sample plate and fixed with tape. The equipment syringe filled with distilled water was installed to stand vertically. 1 µl was deposited on the membrane surface. The CA was measured at 3 different points on each membrane sample.

To study the mean flow pore size, the bubble pressure point and porosity of the membranes, a capillary flow porometer (model no: CFP-1200-AEXL) from PMI Porous Materials Inc., was used. Wet-up/dry-down mode was used for the test on flat sheet membranes with the diameter of

about 22 mm. In order to wet the samples, before running the experiments, one side of the membranes was filled with Gal Wick liquid with surface tension of 15.9mN/m. Each experiment was repeated at least 3 times and the average was calculated.

Thermo gravimetric (TG) analysis of the samples (10-15mg) was performed on a Mettler-Toledo thermal gravimetric analyser at temperature range of 30-500^{0}C with a heat ramping rate of 10°C min^{-1} under nitrogen atmosphere.

The mechanical property of the membrane was studied using an Instron universal materials testing machine (Model 3366). The membrane samples (5 numbers) of length 100 mm, Thickness 0.1mm and width 10mm were used for the test.

Raman spectroscopic measurements were carried out using a Micro Raman spectrometer (Renishaw, system 100) in the range of 3000 to 500 cm^{-1}. The laser spot size was 0 to 250 µm and the excitation was 514 nm. An integration time of 30 s was chosen for each measurement to achieve spectra with good counting rates.

The pure water permeability of the control PANCMA and the G-PANCMI membrane was measured by using cross flow filtration system. A membrane with the total effective membrane area of 120cm^2 (8cm x 20cm) was used to fabricate the membrane module. The two edges of the membrane module were sealed by using epoxy glue while keeping the lumen open on one side to collect the permeate water. The developed membrane module was mounted into the filtration system. Cross-flow ultrafiltration experiments were carried out at 1bar feed pressure. The permeation was collected in a beaker mounted on an electronic balance. After compaction, the pure water flux (Jw) was determined. The filtration experiment was repeated for 3 times with 3 membrane samples and the average was reported

A long term filtration test was carried out by using 10ppm BSA solution. Cross-flow ultrafiltration experiments under constant pressure mode were carried out on the control (PANCMA) and the G-PANCMI by using the same filtration system. The BSA solution was stirred using electrical stirrer to get homogenous feed water and was then pumped through membrane (area 120cm^2) at 1bar pressure. The feed at room temperature was pumped through the membrane at a rate of 2.8 lit/min (LPM). The permeation was collected in a vessel mounted on an electronic balance and the flux drop was calculated (using 4 readings per data point). In order to study the filtration efficiency of the membrane, Total organic carbon (TOC) of the feed and permeate was measured using a TOC analyser (TOC-V_{CSH} instrument from Shimadzu (Catalytic oxidation method) and the rejection percentage was calculated.

Synthesis of functionalized xGnP: 1 gram of the pristine xGnP was refluxed with an excess of acid mixture (H_2SO_4/HNO_3, 3:1) for 12 hours to introduce the acid and hydroxyl functionality on to the graphene surfaces. After successful oxidation, the functionalized xGnP was centrifuged, filtered and washed with excess water until the pH of the wash water was neutral. After thorough drying, the acid functionalized xGnP was further refluxed with 150ml of thionyl chloride at 80^{o}C for 24 hours. The excess thionyl chloride post-reaction was filtered off before 150ml of ethylene diamine was added to the reaction vessel operating under reflux for another 24hours. The amine functionalized xGnP was finally separated out by centrifugation and washed with excess ethanol to remove the unreacted reagents. Figure 1 (a) shows the schematic representation of the synthesis of functionalized graphene nanoplatelets.

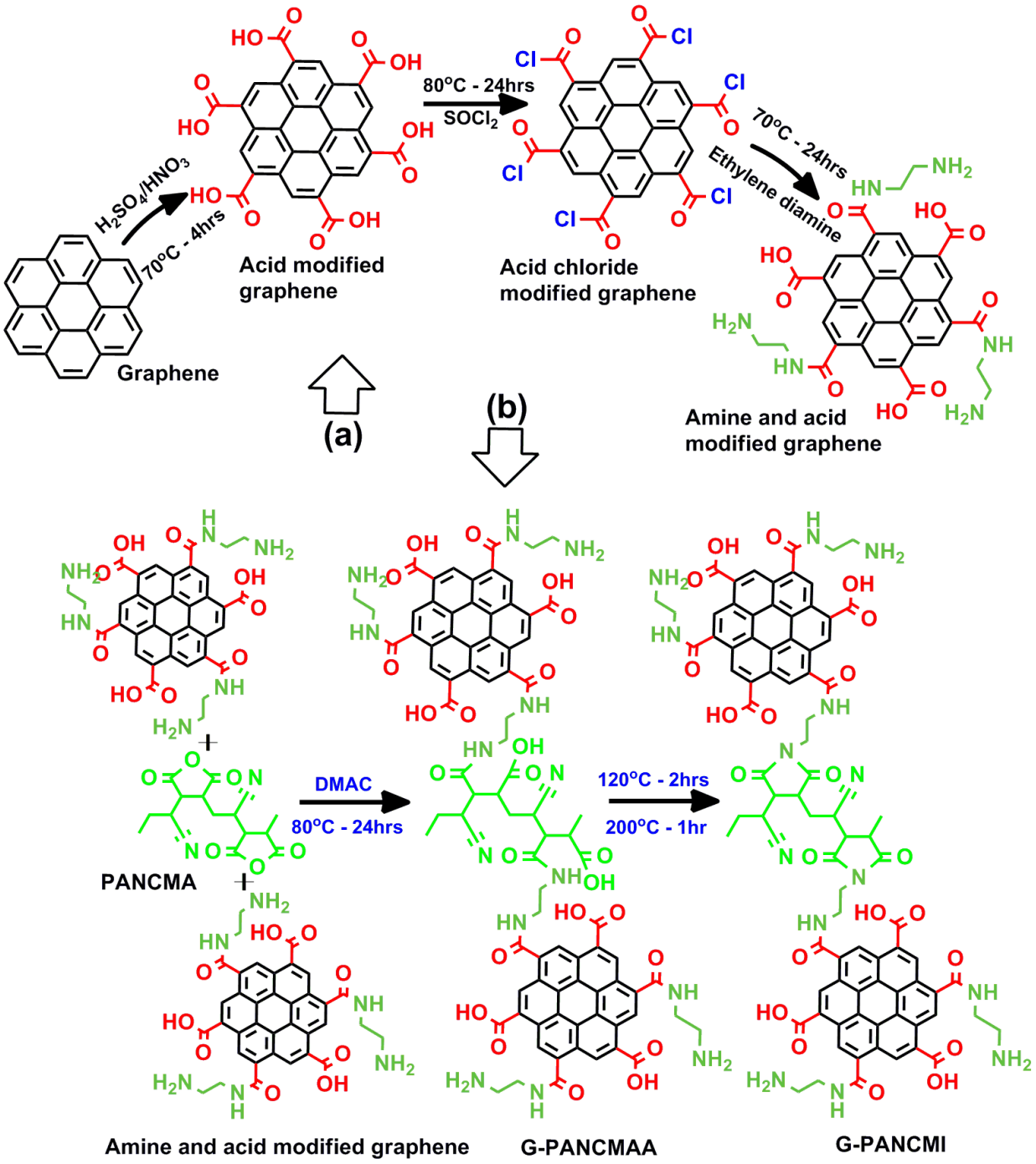

Figure 1: Synthesis of functionalized graphene nanoplatelets (a) Synthesis of G-PANCMI (b)

Synthesis of xGnP grafted PANCMI (G-PANCMI): PANCMA was synthesized as per our previously reported procedure using azobisisobutyronitrile as an initiator [44]. The molecular

weight of the synthesised PANCMA was around 110,000 g/mol as identified by GPC analysis. The synthesized PANCMA was allowed to react for 24 hours with the amine functionalized xGnP in 1:1 ratio (wt %) in 500ml of DMAc at 110^{o}C. The water formed as a result of this condensation reaction was removed by forming an azeotrope with toluene. This reaction leads to the formation of the product in amic acid form. This intermediate product was further subjected to thermal imidisation using a multistage heating of 120^{o}C for 2hours, 200^{o}C for 15mins to obtain the final xGnP grafted PANCMI. Figure 1(b) shows the schematic representation of the synthesis of G-PANCMI.

Membrane preparation: The PANCMA and G-PANCMI ultrafiltration membranes were prepared by the simple phase inversion method [49, 50]. PANCMA / G-PANCMI were used as the base polymers, N-methyl-2-pyrolidone (NMP) was the base solvent, diethylene glycol (DEG) was used as a non-solvent and polyvinylpyrolidone (PVP) was used as an additive (pore forming agent). The composition of the casting solution consists of 21 wt% PANCMA/G-PANCMI, 5 wt% polyvinylpyrolidone (PVP-K-30), 5 wt% Diethylene glycol (DEG), and 69 wt% N-methyl-2-pyrolidone (NMP) respectively. PVP powder was first added into the NMP /DEG mixture in a round bottomed (RB) flask and the solution was stirred by a mechanical stirrer for at least 1-1.5 hours. After complete dissolution of PVP, PANCMA (for control membrane) and G-PANCMI (for modified membrane) were added and allowed to stir at a constant speed of 250~350 rpm for at least 24 hrs at 80^{o}C, to obtain a homogeneous dope solution. The homogeneous G-PANCMI dope solution was used to fabricate ultrafiltration membrane by phase inversion method [49, 50].The prepared membranes were immersed into a post treatment solution of 60% water and

40% glycerine before testing for clean water flux. The set thickness of the membrane was 125 µm and the actual thickness of the membrane after drying was measured to be 100±10 µm.

RESULTS AND DISCUSSION:

Material characterization:

Structural confirmation: The structures of the modified xGnP, PANCMA and G-PANCMI were studied by Fourier transform infrared (FTIR) spectroscopy and the results are presented in Figure 2.

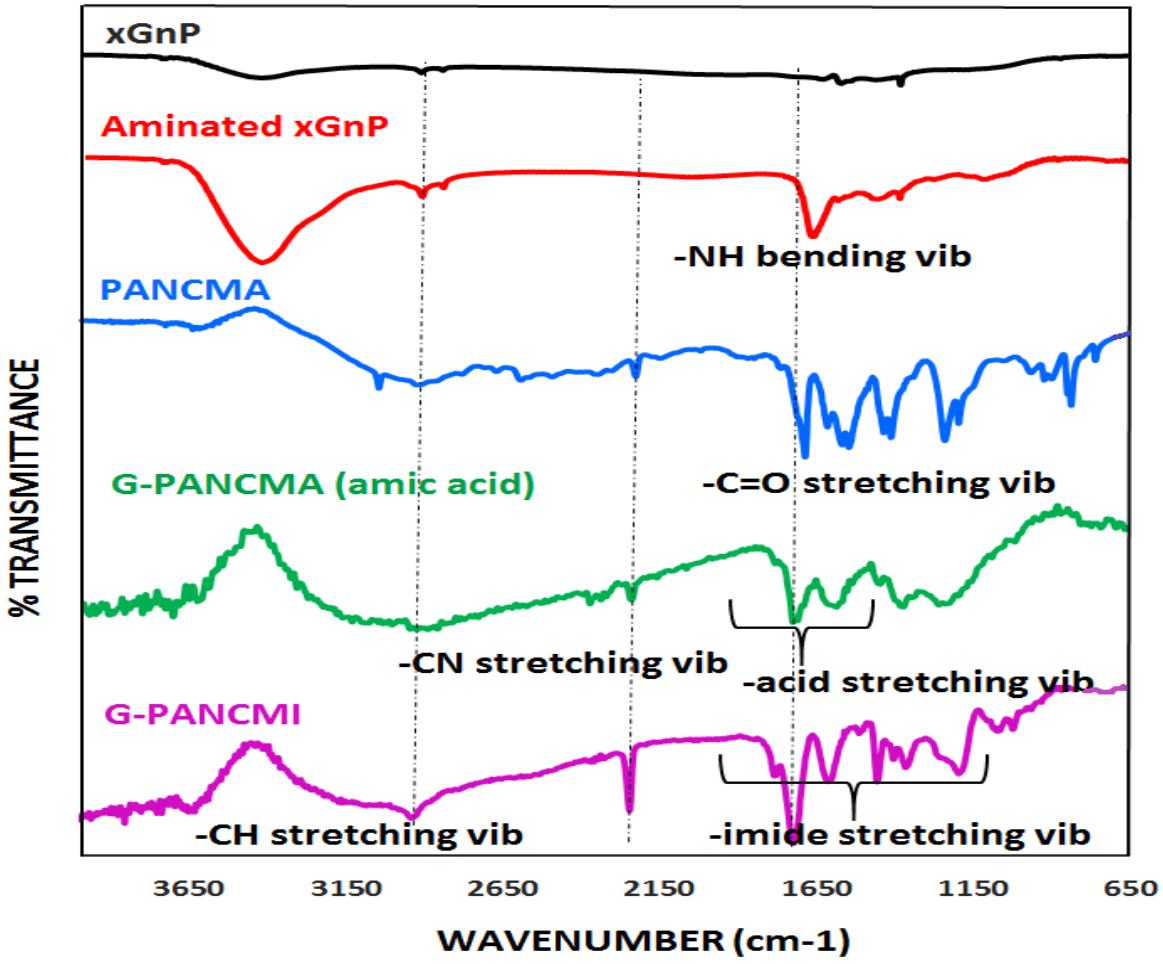

Figure 2: FTIR spectrum of xGnP, amine modified xGnP, PANCMA (anhydride), G-PANCMA (amic acid) and G-PANCMI

The FTIR spectrum of amine modified xGnP shows a broad peak around 3436cm^{-1} for amine stretching vibration (-NH stretching), a small peak at 2915cm^{-1} for the –CH stretching vibrations of the ethylene moiety in ethylene diamine and a sharp and intense peak at 1672 cm^{-1} for –NH bending vibration. This confirms the attachment of ethylene diamine to xGnP. The FTIR spectrum of PANCMA shows a small band at 2972cm^{-1} for the –CH stretching vibration of the –CH_2 groups in maleic anhydride, a sharp peak at 2243cm^{-1} corresponding to the –C-N stretching vibration of nitrile group and bands at 1784cm^{-1} and 1707cm^{-1} for the –C=O stretching vibrations of the anhydride carbonyl groups. The FTIR spectrum of G-PANCMI shows a broad band at 3219cm^{-1} corresponding to the –NH stretching vibration of the diamine moiety, a small peak at 2931cm^{-1} for the –CH stretching vibration, a sharp peak at 2245cm^{-1} corresponding to the –CN stretching vibration of the nitrile group and two sharp peaks at 1770cm^{-1} and 1718cm^{-1}correspondingto the C=O stretching vibrations of the imide carbonyl groups and finally a peak at 1386cm^{-1} for –C-N-C stretching vibration confirming the formation of imide functionality by the attachment of amine modified xGnP to PANCMA.

Figure 3 shows the Raman spectra of xGnP, aminated xGnP and G-PANCMI. All the three compounds exhibited both the D band at around 1350 cm^{-1} and G band at 1590 cm^{-1}. The intensity of D band in aminated xGnP is significantly larger compared to that of the xGnP which is ascribed to the disordered structure of the aminated xGnP by the amine treatment. This D band intensity is further increased in G-PANCMI, which indicates the attachment of PANCMA to the graphene structure. The G-band, which is ascribed to the ordered structure, is also increased due to amination and PANCMA attachment. The attachment of functional groups such as -COOH, -OH,-NH2 and the PANCMA polymer to xGnP is further confirmed by the increase in I_D/I_G (ratio

between the intensity of D band and G band) ratio from 0.23 to 0.56 and to 0.60 for xGnP, aminated xGnP and G-PANCMI respectively.

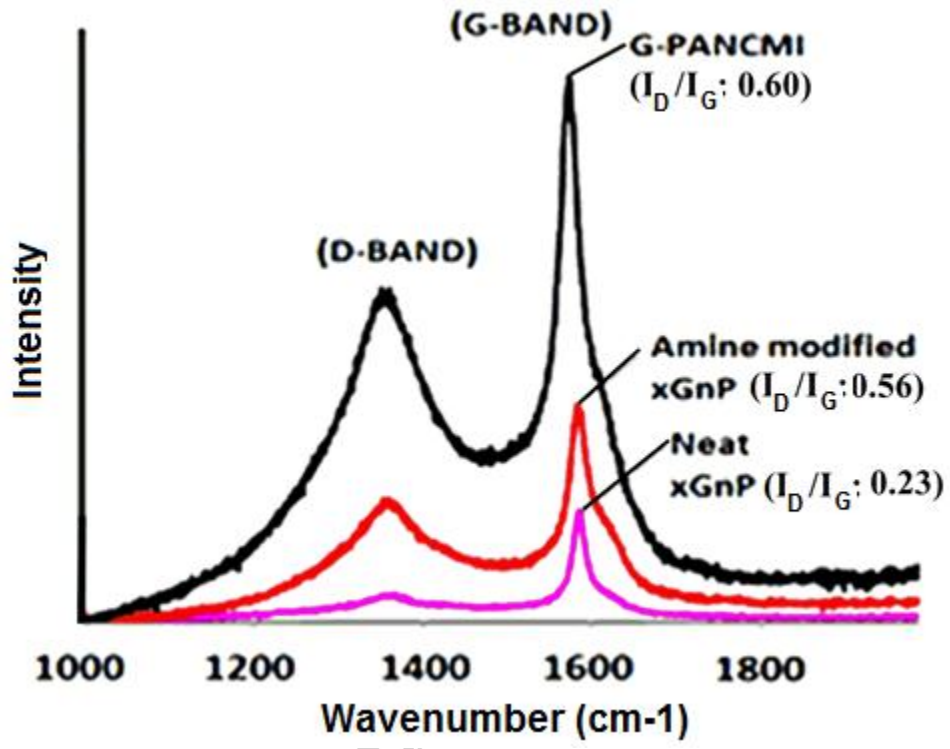

Figure 3: Raman spectroscopy analysis of unmodified graphene, amine and carboxylated graphene and G-PANCMI

The elemental composition of the unmodified, aminated xGnP and G-PANCMI are studied by EDX analysis and the results are tabulated in Table 1. The results shows that, xGnP has a carbon content of 87.6% and Oxygen of 12.4%. On amination, the carbon content decreased to 64.2% with an increase in Oxygen content to 28.1% and with an addition of 7.7% nitrogen content introduced due the amination of xGnP. On grafting this aminated xGnP to PANCMA, the carbon content again increased to 76.7% with an oxygen and nitrogen content of 18.9% and 4.4% respectively.

Table 1: Chemical composition of the unmodified and modified xGnP as studied by EDX analysis

Elements	Atomic weight %		
	xGnP	Aminated xGnP	G-PANCMI
Carbon (C)	87.6	64.2	76.7
Oxygen (O)	12.4	28.1	18.9
Nitrogen (N)	0	7.7	4.4

Figure 4 shows the zeta potential analysis of PANCMA and G-PANCMI. Zeta potential is a key indicator of surface charge as well as the stability of colloidal dispersions. The increased polarity and charge density of the modified graphene are due to the presence of carboxyl, hydroxyl and amine functional groups [20, 24] which increases the negative charge of the polymer. It is also observed that, at normal pH (of around 6-7), the G-PANCMI is more stable in dispersion than PANCMA as it exhibits high negative potential of about -40mv at this pH.

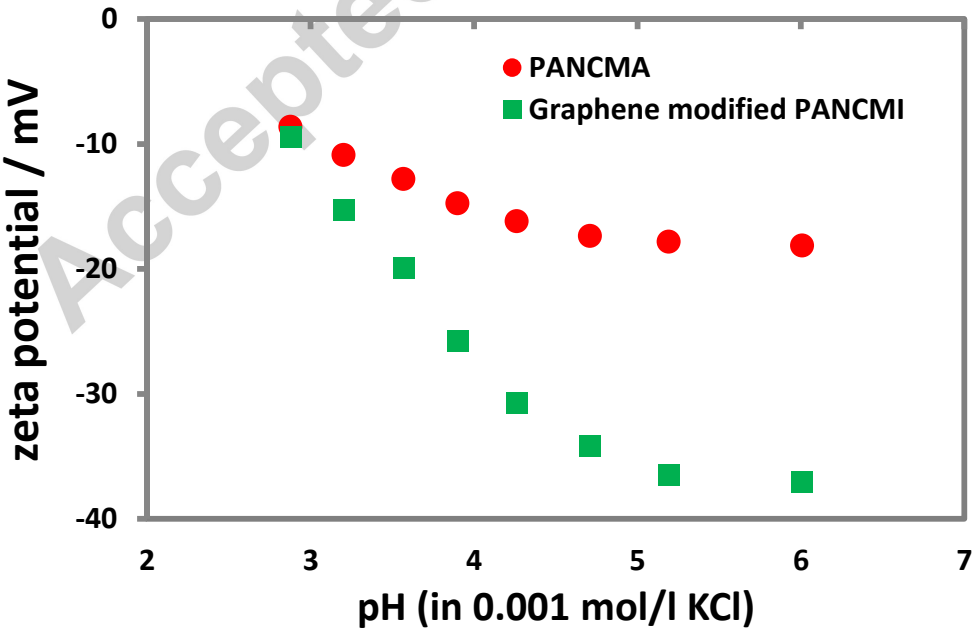

Figure 4: Zeta potential analysis

The differences in thermal stability of PANCMA and G-PANCMI are highlighted in Figure 5a. Compared to PANCMA, G-PANCMI shows excellent thermal stability. There is a slight weight loss at about 90°C for PANCMA, which may be due to loss of solvent or water molecules adsorbed onto it. The drastic weight loss for PANCMA occurs at about 190°C showing the complete degradation of PANCMA. In sharp contrast, G-PANCMI shows greater thermal stability up to a temperature of 400^{o}C, confirming the improved thermal properties due to the presence of xGnP in the polymer matrix.

. The mechanical properties of PANCMA and G-PANCMI are presented in Figure 5b. The results shows that, the grafting of graphene to the PANCMA matrix increases the tensile strength of the matrix. The maximum load for PANCMA was 2.17Mpa and the maximum load for G-PANCMI was 2.91Mpa. The maximum load bearing capacity for G-PANCMI membrane increased by 34% compared to the control PANCMA membrane. The percentage elongation also showed a similar trend as that of tensile strength. The elongation at break for PANCMA was found to be 5.94% and for G-PANCMI, it was observed to be 14.88%. The incorporation of graphene into the PANCMA matrix increased the elongation percentage by 150% compared to PANCMA membrane. Incorporation of graphene nanofillers are known to increase the mechanical strength of the polymer matrix. In this study, since the functionalised xGnP was chemically linked to the polymer matrix, the dispersion of these xGnP in the polymer matrix was good and this led to the increase in the mechanical stability of the G-PANCMI membrane.

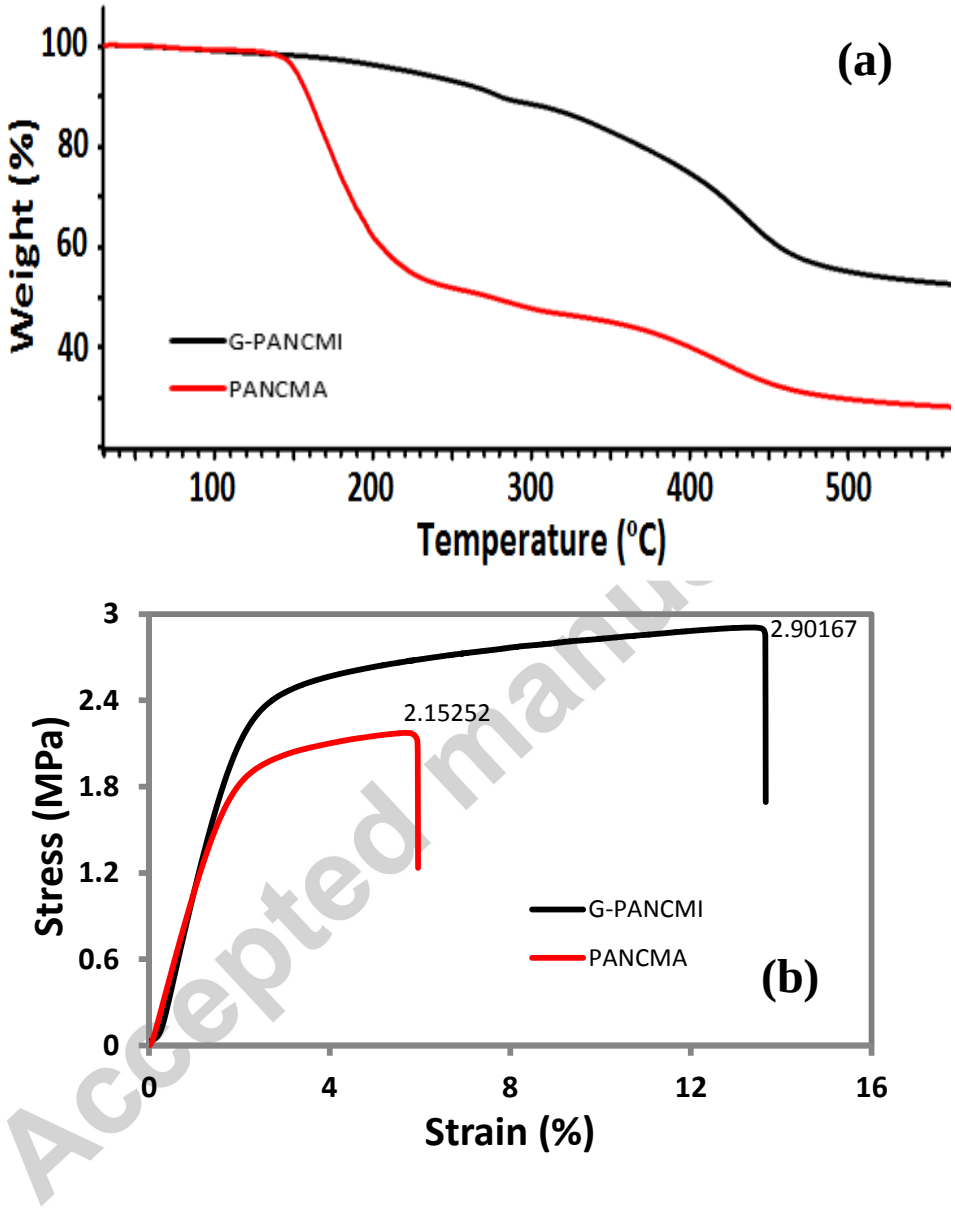

Figure 5: Thermal (a) and mechanical (b) properties of PANCMA and G-PANCMI membranes

Membrane characterization: In order to evaluate the hydrophilicity of the ultra-wetting graphene based membrane, the prepared membranes were tested for their water contact angle (CA_w) and the data are presented in Figure 6a. It is observed that the water contact angle of the G-PANCMI

membrane is reduced to zero (ultra-wetting level) which is 100% lower than that of the PANCMA membrane (average CA_w of PANCMA membrane is 63.3º). The contact angle reduction for the G-PANCMI membrane is due to the presence of highly hydrophilic carboxyl (-COOH), hydroxyl (OH) and amine ($-NH_2$) functional groups on the surface of the graphene Nano sheets attached G-PANCMI. In recent studies, these functional groups have been shown to give similar significant improvements in the hydrophilicity of polymeric membranes [25, 43-46]. The contact angle reduction with time was also evaluated for both the PANCMA and G-PANCMI membranes and the data are presented in Figure 6b. The CA_w of G-PANCMI membrane is reduced to zero within one second (as it is difficult to take readings manually within a second, the images were video recorded for subsequent analysis), whereas PANCMA membrane took 420 seconds to reach <5º. The rapid reduction in contact angle of G-PANCMI membrane further confirmed its ultra-wettability of the modified graphene.

As the dispersibility of the xGnP attached to the polymer is critical to the fabrication of the water filtration membrane by phase inversion method, this parameter was visually evaluated for xGnP and G-PANCMI. 1% solutions of xGnP and G-PANCMI in DMAc were prepared in 50 ml glass bottles and ultrasonicated for 1 hr at 37 kHz. The ultrasonicated solutions were allowed to settle at a constant position at room temperature with relative humidity of 65-70%. Photos were captured 1 hour after ultrasonification and at every subsequent 24 hrs up to 120 hrs. The photos are presented in Figure 6c. The images clearly show that the xGnP completely settles down within a few hours whereas the G-PANCMI remains dispersed, proving that the modified xGnP is more stable in solution for more than 120 hrs. This behaviour of high dispersibility is due to the increased polarity and charge density of the surface of modified graphene containing carboxyl, hydroxyl and amine functional groups [20, 24].

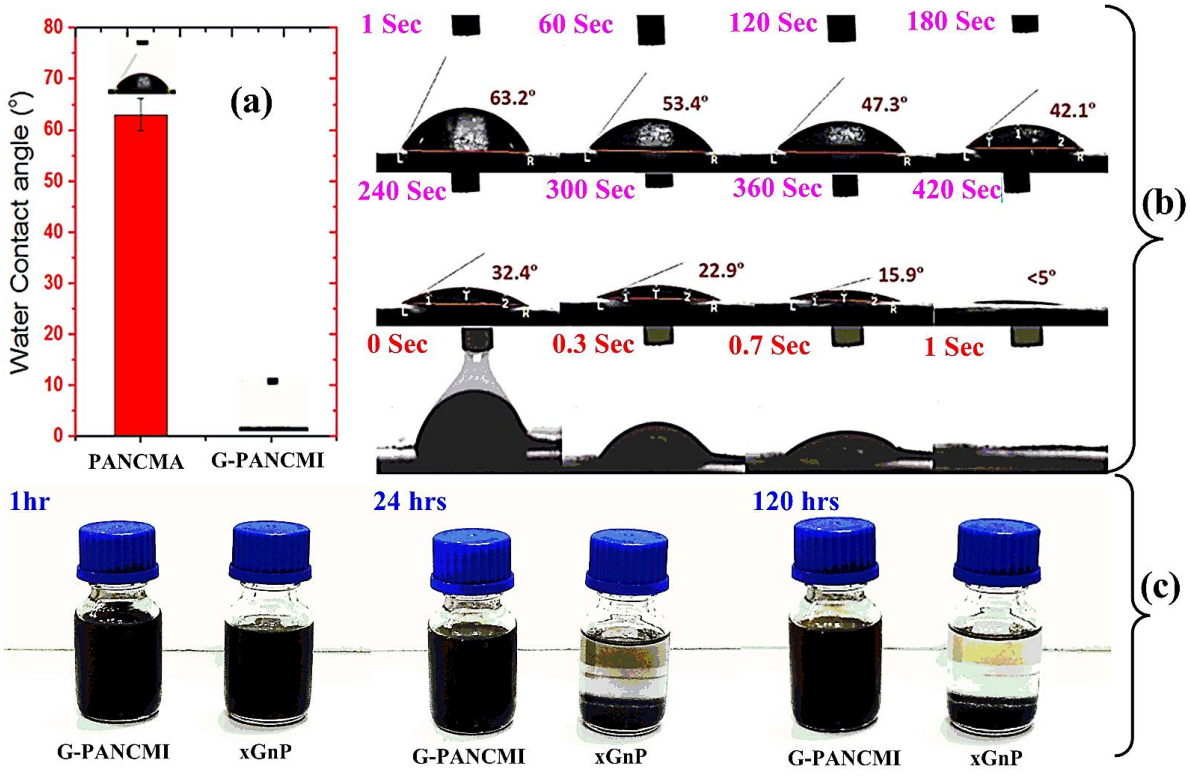

Figure 6: Average water contact angle (a), water contact angle reduction of the PANCMA and G-PANCMI membranes with time (b) and the dispersibility or stability of the unmodified (xGnP) and modified graphene (G-PANCMI) in solution with time (c).

The surface morphology and cross section of the PANCMA and ultra-wetting graphene based G-PANCMI membranes were examined using SEM (Figure 7). Although both membranes had an average thickness of 100µm, they exhibited different internal structures depending on their composition. The PANCMA membrane shows the presence of a large number of macro voids in its internal structure, whereas the ultra-wetting graphene modified G-PANCMI membranes is populated with more sponge-like structures in the cross section next to the internal surface. The presence of highly hydrophilic amine, hydroxyl and carboxylic groups in the ultra-wetting graphene increases the viscosity and reduces the non solvent influx and solvent out flux during phase inversion. This increase in coagulation will slow down the non-solvent/solvent exchange.

As a result, less water will be drawn into the membrane, reducing the macro voids in the ultra-wetting graphene modified G-PANCMI membranes [43, 44, 51].A macro voids free sponge-like structure helps to enhance the porosity, water permeability and selectivity of the membrane [52-54]. Moreover, an even distribution of ultra-wetting graphene nano sheets was observed in the outer surface SEM image of the G-PANCMI membrane. Also, the actual G-PANCMI membrane is black whereas the PANCMA membrane still remains white in colour.

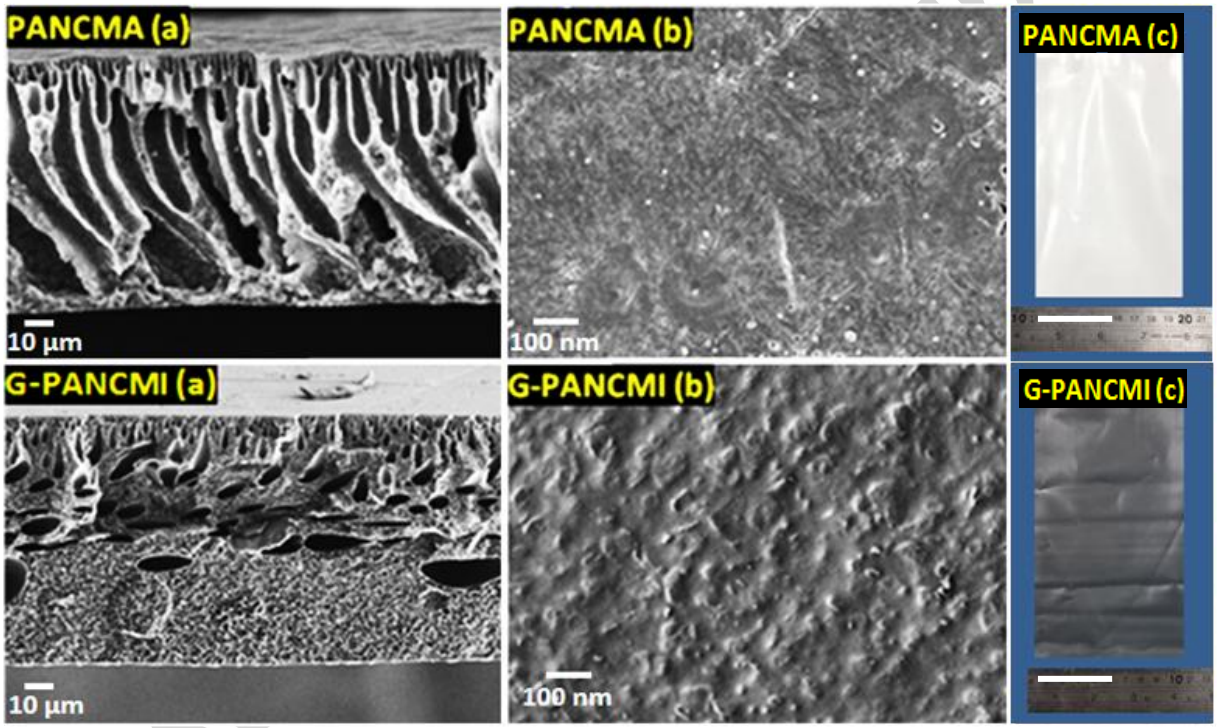

Figure 7: SEM images of PANCMA and G-PANCMI membranes (a) Cross section (b) Outer surface (c) Actual image of synthesized PANCMA and G-PANCMI membranes

On examination of the average pore size of the PANCMA and G-PANCMI membranes, no significant difference is observed. The average pore size of PANCMI based membrane sample is 0.08 ± 0.02µm and 0.07 ± 0.02µm for the G-PANCMI based membrane.

Performance evaluation: The prepared PANCMA and G-PANCMI membranes were tested to evaluate the pure water permeability by cross flow filtration method [43, 44] at constant feed water pressure of 100 kPa and the data are presented in Figure 8a. The PANCMA membrane gave a pure water permeability of 435± 14 $L/m^2/h/bar$. Even though the pore size is similar for both membranes, the G-PANCMI membrane gave higher pure water permeability of 978± 27 $L/m^2/h/bar$ which is around 126% higher compared to the PANCMA membrane. This increase in pure water permeability is due to the increase in hydrophilicity or wettability of the membrane by carboxylic, hydroxyl and amine functional groups which are attached to the graphene nanosheet [25, 43-46].These functional groups attract water towards the membrane surface by inter molecular hydrogen bonding which leads to an increase in permeability [25, 43, 47, 48].

Fouling evaluation using Bovine Serum Albumin (BSA) solution: To evaluate the antifouling efficiency of the membrane, a 9hrs filtration test was conducted using 10ppm BSA in DI water as a feed solution. The results are summarized in Figure 8b. It is observed that the G-PANCMI membrane gives a more stable flux compared to PANCMA membrane samples. Figure 8c shows the normalized permeability or flux drop over time. The flux drop for the G-PANCMI membrane is only 12.3% of the initial flux after 9hrs protein separation whereas the PANCMA membrane's flux drop is 64.3% for the same duration of operation. The obtained results highlight that the presence of negatively charged –COOH and $–NH_2$ in the ultra-wetting graphene based G-PANCMI membrane can best repel the protein from the surface of the membrane.

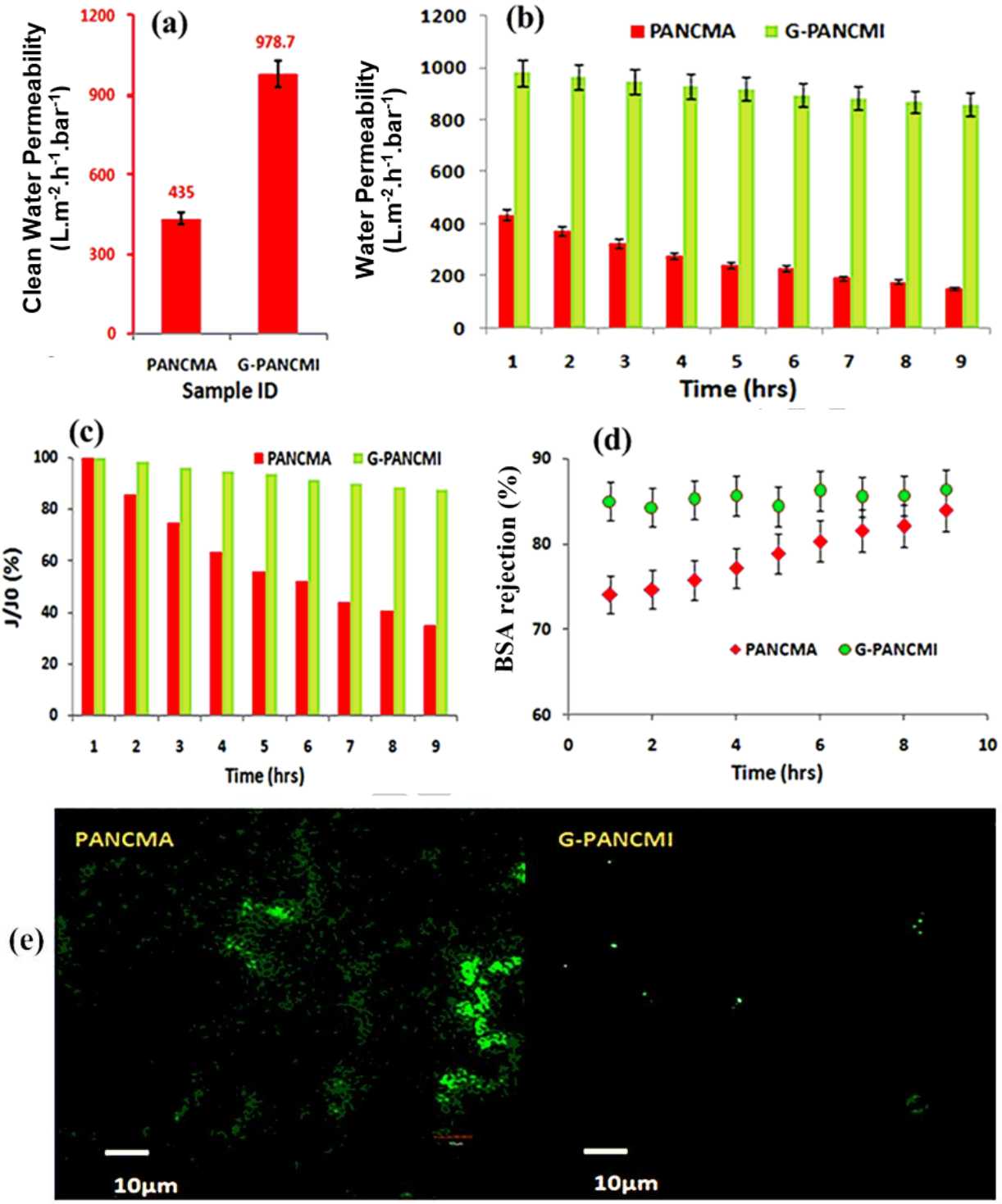

Figure 8:Pure water permeability at 1bar feed pressure (a), water permeability during long time run with 10ppm BSA solution at 1bar feed pressure (b), normalized water permeability for the BSA solution separation during long time run (c), BSA protein (TOC) removal efficiency in % (d) and confocal lacer analysis of the membrane after protein filtration (e).

In order to evaluate the BSA rejection and the filtration efficiency of the membrane, the total organic carbon (TOC) of the feed BSA solution and permeate water were measured. Four samples were collected every 60mins with 15mins frequency and the TOC was measured in order to get the average TOC removal over time. Percentage of TOC rejection was calculated and presented in Figure 8d. From the experimental data, it is found that the TOC removal of the G-PANCMI membrane is also higher and more stable compared to PANCMA membrane. This result also confirms the increased hydrophilicity or wettability of the ultra-wetting graphene based G-PANCMI membranes by negatively charged $–NH_2$ and -COOH on the membrane surface. Recent studies have also shown that the negative surface charge of the membrane prevents the deposition of the negatively charged colloidal particles such as proteins, lipids and amino acids etc., on the membrane surface by electrostatic repulsion, which could slow down or reduce the membrane fouling [43-46]. A similar effect is also apparent in the present work, as depicted in the illustration shown in Figure: 9 below.

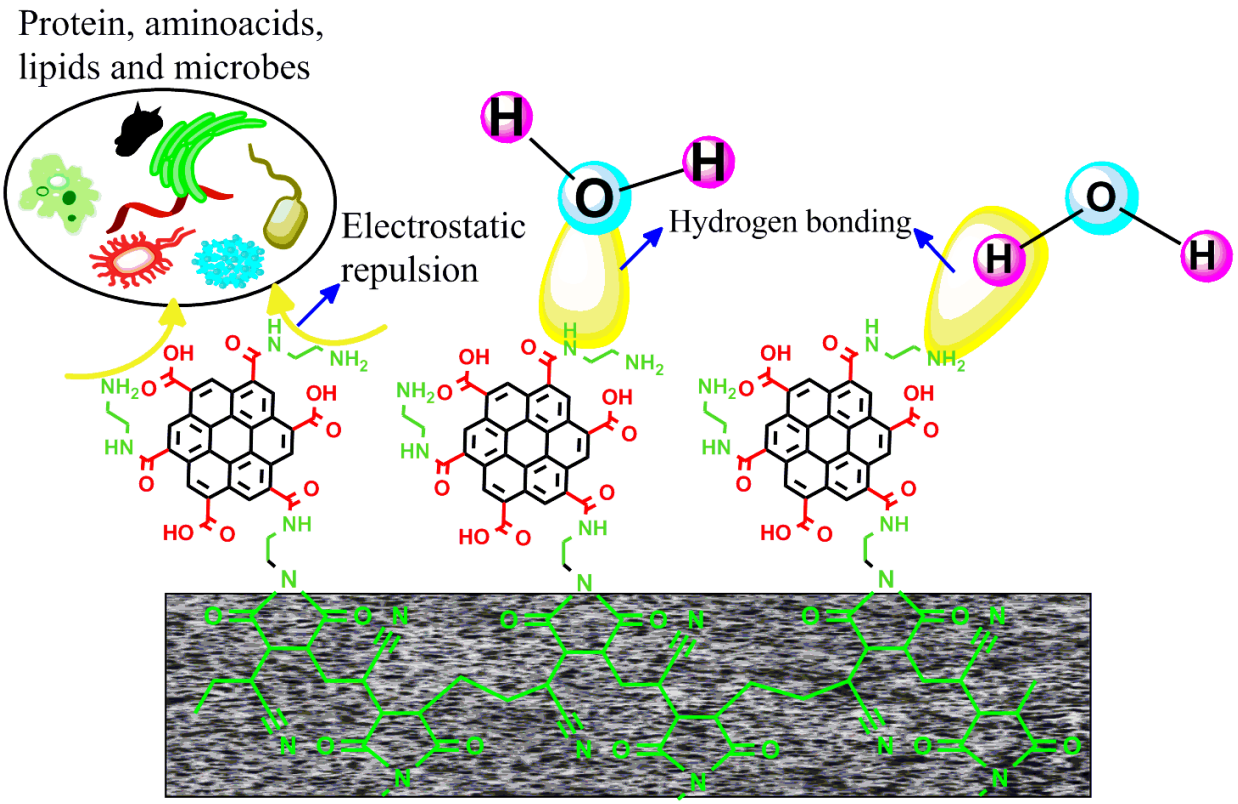

Figure 9. Schematic representation of hydrogen bonding and protein repulsion of the novel membrane

The electrostatic repulsion between the membrane surface and protein and hydrogen bonding between H_2O and $–NH_2$ and –COOH of the G-PANCMI membrane are also highlighted in the graphical abstract. On a related note, it is interesting to see from Figure 8d that the increase in TOC removal efficiency of the control PANCMA membrane with time may be due to the pore constriction/pore blocking or development of fouling on the membrane surface [55]. A confocal lacer scanning (CLSM) analysis was conducted on the membrane samples to evaluate the protein absorption on the membrane surface and the images are presented in Figure 8e. From the images it can be further confirmed that the protein adsorption on the G-PANCMI membrane surface can be negligible in contrast to the relatively high protein adsorption on the PANCMA membrane. The drop in permeability and the improvement in the TOC rejection of the PANCMA membrane

can also be due to the membrane compaction. However, the confocal study clearly shows that, the deposition of BSA on the surface of PANCMA membrane is more than that of G-PANCMI membrane. This result indicates that even if there is possible membrane compaction, fouling of PANCMA membrane is the prime reason for the flux reduction. Finally the performance of the ultra-wetting graphene based membrane was compared against different current state of art polymer-graphene oxide (GO) composite ultrafiltration membranes in terms of permeability and BSA rejection and the data are presented in Figure 10.

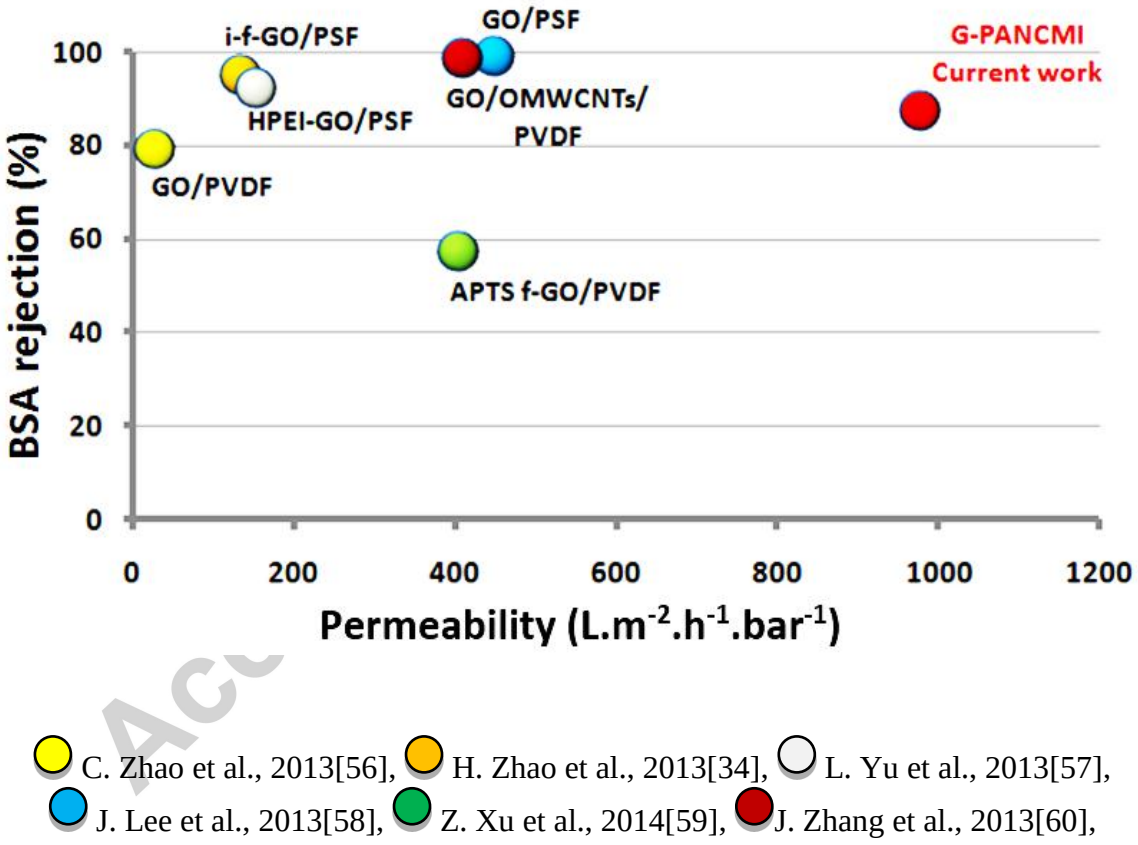

Figure 10: Comparison of the performance of the ultra-wetting graphene based membrane against different current state of art polymer-graphene oxide (GO) composite ultrafiltration membranes in terms of permeability and BSA rejection

From the data it can be easily identified that the ultra-wetting graphene based membrane gives at least 2 times higher permeability compared to the best performing current state of art membranes

without much change in the selectivity [34, 56-60]. Based on our findings, we conclude that the ultra-wetting graphene offers the distinct potential to be an ideal material with significantly improved properties for new generation water filtration membranes.

CONCLUSION:

In this work, we have devised a simple and feasible fabrication method to bring the high end nanocarbon based material graphene to real downstream application. In order to achieve this objective, the wettability of graphene was increased to an ultra-wetting level by incorporating amine and carboxyl functionality onto the graphene. The amine and carboxylated graphene was then covalently attached to a polymer matrix (G-PANCMI) to fabricate ultrafiltration membrane. The characterization of the modified supported graphene based membrane indicates that significantly higher hydrophilicity than previously expected is achieved, with the water contact angle reduced to zero. The ultra-wetting graphene increases the water permeability of the membrane by 126% without any changes in the selectivity. Based on our findings, we conclude that the ultra-wetting graphene will be an ideal material for new generation water filtration membranes.

ACKNOWLEDGEMENT:

This work was supported from funding provided by Ministry of Education, Singapore under the Innovation Fund. The authors also gratefully acknowledge the support from Newcastle University, United Kingdom and Environmental & Water Technology Centre of Innovation (EWTCOI), Ngee Ann Polytechnic, Singapore for the NU-Poly-SIT scholarship awarded to J.A.P.

REFERENCE:

[1] Novoselov KS, Geim AK, Morozov SV, Jiang D, Zhang Y, Dubonos SV, et al. Electric field effect in atomically thin carbon films. Science. 2004;306:666-9.

[2] Zhu Y, Murali S, Stoller MD, Ganesh KJ, Cai W, Ferreira PJ, et al. Carbon-based supercapacitors produced by activation of graphene. Science. 2011;332:1537-41.

[3] Lee C, Li Q, Kalb W, Liu XZ, Berger H, Carpick RW, et al. Frictional characteristics of atomically thin sheets. Science. 2010;328:76-80.

[4] Chen S, Brown L, Levendorf M, Cai W, Ju SY, Edgeworth J, et al. Oxidation resistance of graphene-coated Cu and Cu/Ni alloy. ACS nano. 2011;5:1321-7.

[5] Kim KS, Lee HJ, Lee C, Lee SK, Jang H, Ahn JH, et al. Chemical vapor deposition-grown graphene: the thinnest solid lubricant. ACS nano. 2011;5:5107-14.

[6] Prasai D, Tuberquia JC, Harl RR, Jennings GK, Rogers BR, Bolotin KI. Graphene: corrosion-inhibiting coating. ACS nano. 2012;6:1102-8.

[7] Garaj S, Hubbard W, Reina A, Kong J, Branton D, Golovchenko JA. Graphene as a subnanometre trans-electrode membrane. Nature. 2010;467:190-3.

[8] O'Hern SC, Stewart CA, Boutilier MS, Idrobo JC, Bhaviripudi S, Das SK, et al. Selective molecular transport through intrinsic defects in a single layer of CVD graphene. ACS nano. 2012;6:10130-8.

[9] Rafiee J, Mi X, Gullapalli H, Thomas AV, Yavari F, Shi Y, et al. Wetting transparency of graphene. Nature materials. 2012;11:217-22.

[10] Li Z, Wang Y, Kozbial A, Shenoy G, Zhou F, McGinley R, et al. Effect of airborne contaminants on the wettability of supported graphene and graphite. Nature materials. 2013;12:925-31.

[11] Ruan M, Hu Y, Guo Z, Dong R, Palmer J, Hankinson J, et al. Epitaxial graphene on silicon carbide: Introduction to structured graphene. MRS Bulletin. 2012;37:1138-47.

[12] Leenaerts O, Partoens B, Peeters FM. Graphene: A perfect nanoballoon. Applied Physics Letters. 2008;93:193107.

[13] Gai J-G, Gong X-L, Wang W-W, Zhang X, Kang W-L. An ultrafast water transport forward osmosis membrane: porous graphene. Journal of Materials Chemistry A. 2014;2:4023-8.

[14] Suk ME, Aluru NR. Water Transport through Ultrathin Graphene. The Journal of Physical Chemistry Letters. 2010;1:1590-4.

[15] Allemann RK, Young NJ, Ma S, Truhlar DG, Gao J. Synthetic Efficiency in Enzyme Mechanisms Involving Carbocations: Aristolochene Synthase. Journal of the American Chemical Society. 2007;129:13008-13.

[16] Konatham D, Yu J, Ho TA, Striolo A. Simulation Insights for Graphene-Based Water Desalination Membranes. Langmuir : the ACS journal of surfaces and colloids. 2013;29:11884-97.

[17] Koenig SP, Wang L, Pellegrino J, Bunch JS. Selective molecular sieving through porous graphene. Nat Nano. 2012;7:728-32.

[18] Taherian F, Marcon V, van der Vegt NFA, Leroy F. What Is the Contact Angle of Water on Graphene? Langmuir. 2013;29:1457-65.

[19] Shih CJ, Wang QH, Lin S, Park KC, Jin Z, Strano MS, et al. Breakdown in the wetting transparency of graphene. Physical review letters. 2012;109:176101.

[20] Dreyer DR, Park S, Bielawski CW, Ruoff RS. The chemistry of graphene oxide. Chemical Society Reviews. 2010;39:228-40.

[21] Loh KP, Bao Q, Eda G, Chhowalla M. Graphene oxide as a chemically tunable platform for optical applications. Nat Chem. 2010;2:1015-24.

[22] Avouris P, Dimitrakopoulos C. Graphene: synthesis and applications. Materials Today. 2012;15:86-97.

[23] Compton OC, Nguyen ST. Graphene Oxide, Highly Reduced Graphene Oxide, and Graphene: Versatile Building Blocks for Carbon-Based Materials. Small. 2010;6:711-23.

[24] Wajid AS, Das S, Irin F, Tanvir Ahmed HS, Shelburne JL, Parviz D, et al. Erratum to 'Polymer-stabilized graphene dispersions at high concentrations in organic solvents for composite production' [Carbon 50 (2012) 526–534]. Carbon. 2012;50:2065.

[25] Jin F, Lv W, Zhang C, Li Z, Su R, Qi W, et al. High-performance ultrafiltration membranes based on polyethersulfone-graphene oxide composites. RSC Advances. 2013;3:21394-7.

[26] Marmur A. Soft contact: measurement and interpretation of contact angles. Soft Matter. 2006;2:12-7.

[27] Rafiee J, Mi X, Gullapalli H, Thomas AV, Yavari F, Shi Y, et al. Wetting transparency of graphene. Nature materials. 2012;11:217-22.

[28] Shih C-J, Wang QH, Lin S, Park K-C, Jin Z, Strano MS, et al. Breakdown in the Wetting Transparency of Graphene. Physical Review Letters. 2012;109:176101.

[29] Cohen-Tanugi D, Grossman JC. Water Desalination across Nanoporous Graphene. Nano Letters. 2012;12:3602-8.

[30] Sun P, Zhu M, Wang K, Zhong M, Wei J, Wu D, et al. Selective Ion Penetration of Graphene Oxide Membranes. ACS nano. 2013;7:428-37.

[31] Hu M, Mi B. Enabling Graphene Oxide Nanosheets as Water Separation Membranes. Environmental Science & Technology. 2013;47:3715-23.

[32] Qiu S, Wu L, Pan X, Zhang L, Chen H, Gao C. Preparation and properties of functionalized carbon nanotube/PSF blend ultrafiltration membranes. Journal of Membrane Science. 2009;342:165-72.

[33] Maphutha S, Moothi K, Meyyappan M, Iyuke SE. A carbon nanotube-infused polysulfone membrane with polyvinyl alcohol layer for treating oil-containing waste water. Scientific reports. 2013;3:1509.

[34] Zhao H, Wu L, Zhou Z, Zhang L, Chen H. Improving the antifouling property of polysulfone ultrafiltration membrane by incorporation of isocyanate-treated graphene oxide. Physical Chemistry Chemical Physics. 2013;15:9084-92.

[35] Liu T, An Q-F, Zhao Q, Wu J-K, Song Y-H, Zhu B-K, et al. Synergistic strengthening of polyelectrolyte complex membranes by functionalized carbon nanotubes and metal ions. Sci Rep. 2015;5.

[36] Vickery JL, Patil AJ, Mann S. Fabrication of Graphene–Polymer Nanocomposites With Higher-Order Three-Dimensional Architectures. Advanced Materials. 2009;21:2180-4.

[37] Yang L, Tang B, Wu P. UF membrane with highly improved flux by hydrophilic network between graphene oxide and brominated poly(2,6-dimethyl-1,4-phenylene oxide). Journal of Materials Chemistry A. 2014;2:18562-73.

[38] Li G, Wang X, Tao L, Li Y, Quan K, Wei Y, et al. Cross-linked Graphene membrane for High-performance Organics separation of Emulsions. Journal of Membrane Science.

[39] Liu G, Jin W, Xu N. Graphene-based membranes. Chemical Society Reviews. 2015;44:5016-30.

[40] Shao L, Chang X, Zhang Y, Huang Y, Yao Y, Guo Z. Graphene oxide cross-linked chitosan nanocomposite membrane. Applied Surface Science. 2013;280:989-92.

[41] Singh SK, Singh MK, Kulkarni PP, Sonkar VK, Grácio JJA, Dash D. Amine-Modified Graphene: Thrombo-Protective Safer Alternative to Graphene Oxide for Biomedical Applications. ACS nano. 2012;6:2731-40.

[42] Cao L, Sun Q, Gao Y, Liu L, Shi H. Novel acid-base hybrid membrane based on amine-functionalized reduced graphene oxide and sulfonated polyimide for vanadium redox flow battery. Electrochimica Acta. 2015;158:24-34.

[43] Prince JA, Bhuvana S, Anbharasi V, Ayyanar N, Boodhoo KVK, Singh G. Self-cleaning Metal Organic Framework (MOF) based ultra filtration membranes - A solution to bio-fouling in membrane separation processes. Sci Rep. 2014;4.

[44] Prince JA, Bhuvana S, Boodhoo KVK, Anbharasi V, Singh G. Synthesis and characterization of PEG-Ag immobilized PES hollow fiber ultrafiltration membranes with long lasting antifouling properties. Journal of Membrane Science. 2014;454:538-48.

[45] Knoell T, Safarik J, Cormack T, Riley R, Lin SW, Ridgway H. Biofouling potentials of microporous polysulfone membranes containing a sulfonated polyether-ethersulfone/polyethersulfone block copolymer: correlation of membrane surface properties with bacterial attachment. Journal of Membrane Science. 1999;157:117-38.

[46] Khulbe KC, Feng C, Matsuura T. The art of surface modification of synthetic polymeric membranes. Journal of Applied Polymer Science. 2010;115:855-95.

[47] Hoek EMV, Kaner RB, GUILLEN GR, Farrell TP. Polyaniline membranes, uses, and methods thereto. Google Patents; 2014.

[48] Martín A, Arsuaga JM, Roldán N, de Abajo J, Martínez A, Sotto A. Enhanced ultrafiltration PES membranes doped with mesostructured functionalized silica particles. Desalination. 2015;357:16-25.

[49] Prince JA, Rana D, Singh G, Matsuura T, Jun Kai T, Shanmugasundaram TS. Effect of hydrophobic surface modifying macromolecules on differently produced PVDF membranes for direct contact membrane distillation. Chemical Engineering Journal. 2014;242:387-96.

[50] Matsuura T. Synthetic Membranes and Membrane Separation Processes: CRC Press December 17, 1993

[51] Khayet M, Feng CY, Khulbe KC, Matsuura T. Preparation and characterization of polyvinylidene fluoride hollow fiber membranes for ultrafiltration. Polymer. 2002;43:3879-90.

[52] Sukitpaneenit P, Chung T-S. High Performance Thin-Film Composite Forward Osmosis Hollow Fiber Membranes with Macrovoid-Free and Highly Porous Structure for Sustainable Water Production. Environmental Science & Technology. 2012;46:7358-65.

[53] Baker R. Membrane technology and applications. Wiley. 2004.

[54] Weber M, Maletzko C, Widjojo N, ZHONG P, Chung TS. Ultrafiltration membranes fabricated from sulfonated polyphenylenesulfones. Google Patents; 2013.

[55] Katsoufidou K, Yiantsios SG, Karabelas AJ. Experimental study of ultrafiltration membrane fouling by sodium alginate and flux recovery by backwashing. Journal of Membrane Science. 2007;300:137-46.

[56] Zhao C, Xu X, Chen J, Yang F. Effect of graphene oxide concentration on the morphologies and antifouling properties of PVDF ultrafiltration membranes. Journal of Environmental Chemical Engineering. 2013;1:349-54.

[57] Yu L, Zhang Y, Zhang B, Liu J, Zhang H, Song C. Preparation and characterization of HPEI-GO/PES ultrafiltration membrane with antifouling and antibacterial properties. Journal of Membrane Science. 2013;447:452-62.

[58] Lee J, Chae H-R, Won YJ, Lee K, Lee C-H, Lee HH, et al. Graphene oxide nanoplatelets composite membrane with hydrophilic and antifouling properties for wastewater treatment. Journal of Membrane Science. 2013;448:223-30.

[59] Xu Z, Zhang J, Shan M, Li Y, Li B, Niu J, et al. Organosilane-functionalized graphene oxide for enhanced antifouling and mechanical properties of polyvinylidene fluoride ultrafiltration membranes. Journal of Membrane Science. 2014;458:1-13.

[60] Zhang J, Xu Z, Shan M, Zhou B, Li Y, Li B, et al. Synergetic effects of oxidized carbon nanotubes and graphene oxide on fouling control and anti-fouling mechanism of polyvinylidene fluoride ultrafiltration membranes. Journal of Membrane Science. 2013;448:81-92.

TOC-Art / Graphical abstract

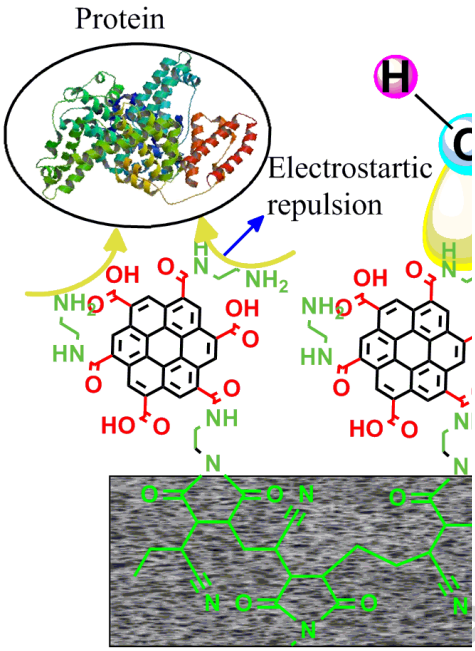

Highlights:

- Graphene was modified with carboxyl, hydroxyl and amine functional groups
- The modified graphene was covalently attached to a polymer matrix (G-PANCMI)
- The novel graphene nanocomposite G-PANCMI was used to fabricate UF membrane
- The water contact angle of the novel membrane was reduced to zero.
- The G-PANCMI increases the water permeability by 126% with stable selectivity